Microstructure and mechanical properties of titanium components fabricated by a new powder injection molding technique

Eric Nyberg[a,*], Megan Miller[b], Kevin Simmons[a], K. Scott Weil[a]

[a]Battelle Memorial Institute, Richland, WA 99352, United States
[b]Currently studying at the University of Alabama, Birmingham, AL, United States

Abstract

A powder injection molding (PIM) binder system has been developed for reactive metals such as titanium that employs an aromatic compound as the primary component to facilitate easy binder removal and mitigate problems with carbon contamination. In the study presented here, we examined the densification behavior, microstructure, and mechanical properties of titanium specimens formed by this process using naphthalene as the principle binder constituent. In general, it was found that tensile strengths could be achieved comparable to wrought titanium in the PIM-formed specimens, but that maximum elongation was less than expected. Chemical and microstructural analyses indicate that this process does not add oxygen to the material, suggesting that the use of higher purity powder and further process optimization should lead to significant improvements in ductility.
© 2005 Published by Elsevier B.V.

1. Introduction

The use of titanium in biomedical applications continues to gain attention because of its unique properties, including high specific strength, low density and lightweight feel, excellent corrosion resistance, and biocompatibility [1,2]. These translate into tremendous clinical advantages in terms of reduced recovery time and rehabilitation and improved patient comfort, making it a nearly ideal material for the development of medical bone reinforcement and replacement products [3–6]. At present however, the fabrication of titanium-based implants is limited to a costly, multi-step process of vacuum arc melting, hot rolling, scale removal, vacuum annealing, machining, and surface treatment. There is an overwhelming need in the industry for an alternative method of titanium manufacture, one that simultaneously reduces the cost and complexity of processing, enhances design flexibility, and improves the biological activity of the implant surface without compromising its structural integ-rity, i.e. its strength, fatigue resistance, and biocompatibility. A leading candidate is powder injection molding (PIM).

PIM is a well-established, cost-effective method of fabricating small-to-moderate size metal components. The process is derived from plastic injection molding and is comprised of four main steps: (1) mixing of metal powder with a polymer binder to form the feedstock, (2) injection of the feedstock mixture into a mold, (3) binder removal (via heat treatment, solubilization, or catalytic decomposition), and (4) sintering or densification [7]. Pellets or granules of the feedstock material are fed into a heated chamber and the resulting melt is forced under pressure into a split-mold cavity where it quickly cools before the mold is opened and the part is ejected onto a conveyor belt or into a storage bin. Use of easily removed fugitive phases in the feedstock mixture and control of the de-binding and sintering treatments allow the porosity of the component to be optimized, affording potential advantages in a number of specialized applications including the design of self-lubricating parts and biomedical implants.

However, while PIM has been used with great success in manufacturing a wide variety of metal products, including those made from stainless steel, nickel-based superalloys,

---

* Corresponding author.
  E-mail address: Eric.Nyberg@pnl.gov (E. Nyberg).

and copper alloys [8–10], it has found far less application with reactive metals, such as titanium, primarily because of problems with interstitial impurities. In particular, high levels of oxygen are often found in inexpensive titanium powder sources. Also, given the high binder loadings generally employed in PIM, carbon can be readily introduced due to insufficient binder removal prior to sintering and/or to deleterious reactions between the decomposing binder, the debinding atmosphere, and the metal phase. Even at low concentration, these impurities can cause severe degradation in the mechanical properties of titanium and its alloys [11].

Earlier investigations on titanium PIM (Ti-PIM) employed the thermoplastic and/or thermoset binder systems typically used in other metal injection molding processes, with these materials constituting ~40–50 vol.% of the feedstock and downstream binder removal taking place via thermal pyrolysis [12–14]. More recently, binders have been designed that are soluble in water or organic solvents and/or contain a catalyst that facilitates in-situ decomposition [15,16]. However, feedstocks that employ these materials still require high binder loadings. As reported previously, an alternate binder system has been developed specifically for injection molding reactive metals such as titanium that utilizes naphthalene as the primary binder component [17,18]. The advantages of this compound are that it melts at relatively low temperature, 81°C, and can be removed via sublimation at temperatures below its melting point. Consequently naphthalene can act both as the binder backbone and as a solvent for additional binder constituents used to improve the mixing properties of the feedstock and the green strength of the molded parts. Here, the as-sintered properties of titanium components fabricated using this process are reported.

2. Experimental methods

To mitigate concerns with high oxygen content, titanium hydride (TiH$_2$; Titanium Systems, Inc.) was used as the titanium powder source in all of the experiments. Several reports suggest that TiH$_2$ self-reduces oxygen impurities during thermal decomposition (around 350°C or higher, depending on the ambient atmosphere) to form metallic
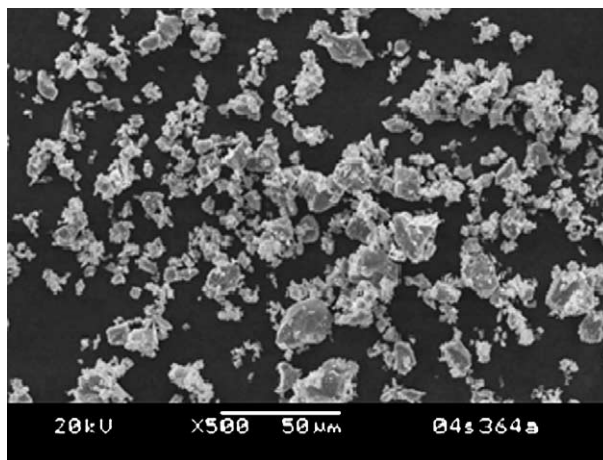

Fig. 1. SEM image of the starting TiH$_2$ powder showing angular particle morphology.

titanium, although the mechanisms for this are not well understood [19,20]. The characteristics of this powder are given in Table 1, and its distinctive angular morphology is shown in Fig. 1. The binder system contained 93 vol.% naphthalene (Aldrich Chemical Co.), 6 vol.% ethylene vinyl acetate (EVA, Microthene MU 763-00; Equistar Chemicals LP) to improve green strength, and 1 vol.% stearic acid (Aldrich Chemical Co.) as a powder surfactant and lubricant. A 50:50 combination of mold release agents Dow Corning DC 20 and Miller-Stephenson Teflon™ was applied to the mold cavities prior to feedstock injection to aid in removing the molded parts.

Cylindrical Ti-PIM tensile bars of the type shown in Fig. 2 were fabricated via the process outlined in Fig. 3. The feedstock mixing and injection molding parameters that were employed are given in Table 2. Feedstock formulations of TiH$_2$ and the premixed binder were prepared by shear mixing in a Haake Rheocord 90 (Thermo Electron Corporation, Waltham, MA) using dual Brabender mixing screws at 85°C. Once the feedstock was well homogenized, as indicated by a drop in the mixing torque to a minimum steady-state value, the mixing bowl was gradually cooled. As this occurred, the mixture began to solidify and under continuous shearing in the mixer, formed a coarse powder (<1–2 mm average particle size) that was used as the PIM feedstock. Molded bars were fabricated by feeding the

Table 1
Powder characteristics for the titanium hydride powder

Powder Type	Titanium Hydride (TiH$_2$)
Vendor	Titanium Systems, Inc.
Tap density, g/cm^3	2.7
BET surface area, m^2/g	0.11
Particle size distribution, μm	
D_{10}	2.39
D_{50}	7.84
D_{90}	19.93
Mean	8.60

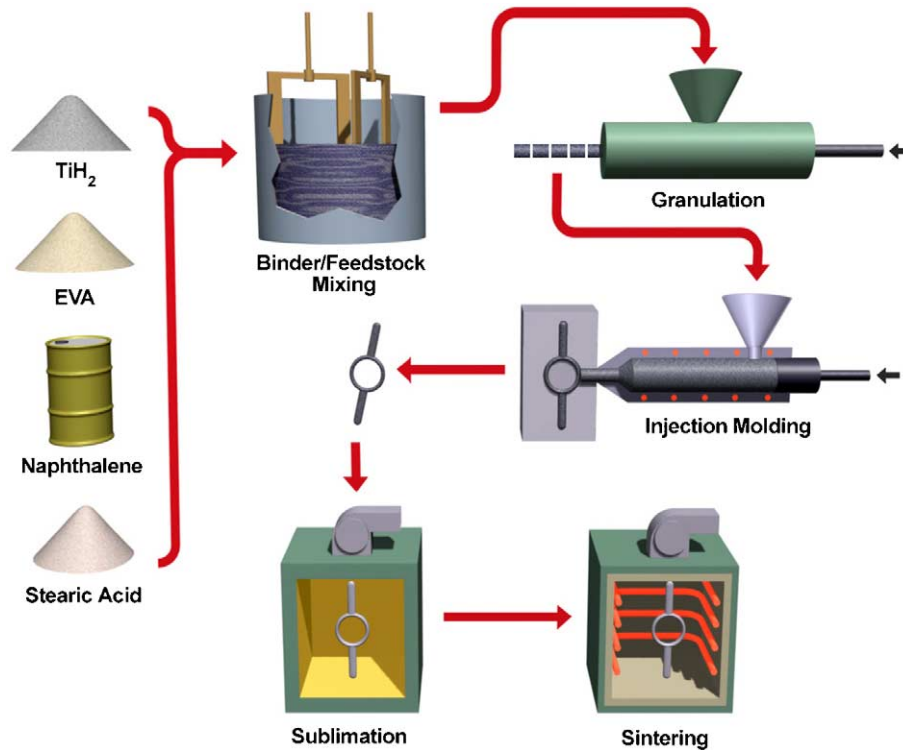Fig. 2. ASTM E8 tensile specimens fabricated by the naphthalene-based Ti-PIM process.

Fig. 3. Flow chart for the naphthalene-based Ti-PIM process.

material into the heated barrel of a 20 MPa injection molder (Crystal Alloy Injectors USA, Minneapolis, MN). The barrel temperature was maintained at an external temperature of 135°C, which was found to be hot enough internally to keep the feedstock sufficiently fluid, and the molten slurry was injected under maximum pressure into an aluminum mold. The mold contained two cylindrical dogbone-shaped cavities (ASTM E8, scaled up to account for maximum part shrinkage of 19% during drying/sintering) each connected on one end to a central 4 mm diameter injection port.

As molded, the tensile specimens measured 5 mm diameter × 40 mm long through the gage length body and 15 mm diameter × 7.62 mm long at each grip end with a 0.8 mm radius at the gage to grip (shoulder) transitions. The naphthalene was removed by sublimation under $\sim 2 \times 10^{-2}$ Torr of vacuum at a 48-h isothermal hold of 75°C. Final removal of the remaining binder and subsequent sintering were conducted in a single-step heat treatment run. Specimens were placed onto a pre-reduced zirconia setter plate, and heat treated in a refractory metal furnace (front loading SinterMaster, Thermal Technology, Inc., Santa Rosa, CA) under a set of conditions determined from previously reported thermal analysis experiments [18]: heat in Ar/2.75% H_2 at 1°C/min to 375°C; hold at 375°C for 3 h; heat at 1°C/min to 750°C, turn off the gas flow, and begin pulling a vacuum on the heating chamber while holding at 750°C for 3 h; continue heating in 10^{-6} Torr vacuum at 5°C/min to a final soak temperature of 1100°C and hold for 4 h; followed by argon assisted convective cooling to room temperature.

Density measurements of the sintered specimens were conducted by simple geometric and weight measurements, as well as by the Archimedes technique using distilled water as the displacement medium. The microstructures of the sintered samples were characterized on polished cross sections using an Olympus BX60 optical light microscope and SZ12 stereo microscope (LECO Corp., St. Joseph, MI) and a JEOL JSM-5900 LV scanning electron microscopy (SEM; JEOL USA, Inc., Peabody, MA) equipped with an Oxford Energy Dispersive X-ray Spectrometer (EDS) system (Oxford Instruments, UK). X-ray diffraction (XRD) analysis was carried out with a Philips Wide-Range Vertical Goniometer (Philips Electronics, Netherlands) and a Philips XRG3100 X-ray Generator over a scan range of 20–80° 2Θ with a 0.04° step size and 2 s hold time. XRD

Table 2
Feedstock mixing and injection molding parameters

Mixing	
Temperature	85°C
Time	10 min
Speed	50 rpm
Blade Type	Brabender
Injection Molding	
External barrel temperature	135°C
Injection pressure	20 Mpa
Feedstock charge	30 g
Resonance time in barrel	30 s
Hold time	45 s
Cycle time	1 min 15 s
Mold temperature	20°C

Table 3
Powder and binder loadings employed in the feedstocks

Volume fraction TiH$_2$ Powder	Powder (wt.%)	Binder (wt.%)
50	80.6	19.4
55	83.5	16.5
60	86.0	14.0
62	87.0	13.0
65	88.4	11.6
67	89.2	10.8
70	90.4	9.6

pattern analysis was conducted using Jade 6+ (EasyQuant) software. Quantitative combustion analyses using the American Society for Testing and Materials standard ASTM D5373 were performed on the raw TiH$_2$ powders and the as-sintered titanium PIM components at Wah Chang Corporation (Albany, OR) to determine the nitrogen, carbon, and oxygen contents prior to and after PIM processing. Tensile testing was performed using an Instron model 4465 test unit (Instron Corporation, Canton, MA) according to the conditions specified by ASTM E8. A constant crosshead speed of 0.25 mm/min was employed.

3. Results

In forming the initial liquid binder, both the EVA and stearic acid appeared to dissolve completely in molten naphthalene, yielding a transparent solution after a few minutes of heating at ∼90°C. Feedstock batches were formulated by adding TiH$_2$ powder as described above to achieve the final loadings given in Table 3. After injection molding and heat treating, specimen density was evaluated as function of TiH$_2$ loading in the initial feedstock material. As shown in Fig. 4, sintered density displays a monotonic increase with increased powder loading. Often these two parameters display little or no correlation in PIM processing [21]. Instead, a strong dependence of part shrinkage on powder loading is typically observed, with changes in specimen volume occurring during both binder removal and sintering. That is, with many thermoplastic and thermoset binder systems, the debound parts tend to achieve approx-
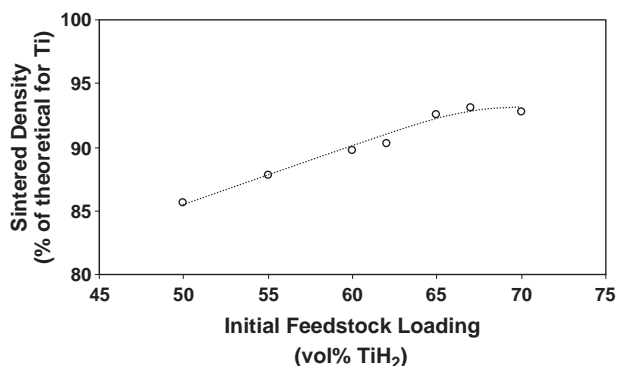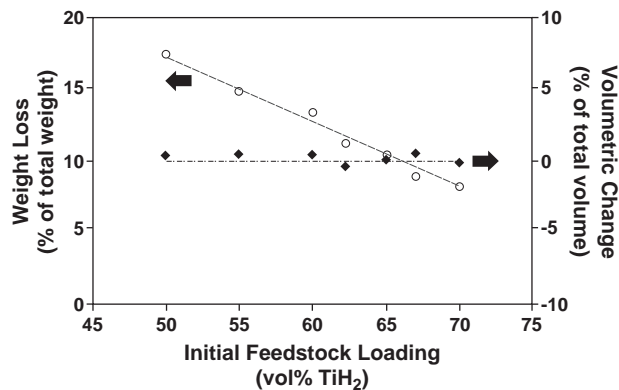

Fig. 5. Weight loss and volumetric change as a function of initial feedstock loading, after sublimation at 75°C for 48 h under ∼2 × 10^{-2} Torr of vacuum.

imately the same pre-sintered density independent of the intial powder loading in the PIM feedstock. However, the amount of volumetric shrinkage is inversely related to powder loading [21]. In the naphthalene based process, the opposite appears to occur. As shown in Fig. 5, even though the specimens lose a significant amount of weight during debinding due to napthalene sublimation, their volumes remain essentially constant. Thus as seen in Fig. 6, the density of the debound part (i.e. green density) increases with increasing powder loading.

A similar phenomenon is observed in supercritical drying. In fact, this drying technique is used to synthesize extremely low density aerogel materials precisely because evaporation takes place with virtually no commensurate change in material volume [22]. The phenomenon is typically attributed to the low surface energies intrinsic to supercritical fluids. Consequently, as the fluid is removed through pores in the drying body, it exerts very little capillary or collapsing force on the remaining solid, subsequently causing little change in the solid's bulk volume during drying. Similarly, sublimation involves low surface energies in the vaporizing "solvent". While this means that part distortion can be mitigated during debinding, it also implies that one must be careful to maximize the initial powder loading in the feedstock to achieve good part
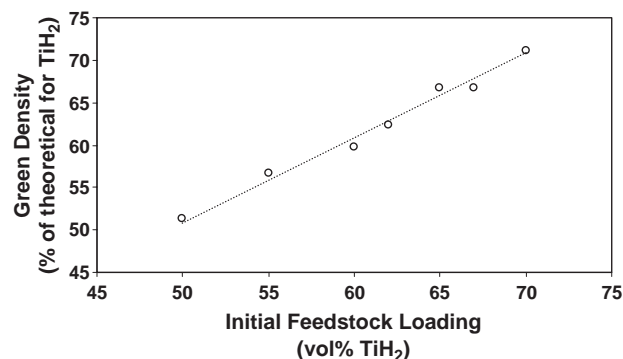

Fig. 4. Sintered density as a function of initial feedstock loading, after heat treating at 1100°C for 4 h under vacuum.

Fig. 6. Green density as a function of initial feedstock loading, after sublimation at 75°C for 48 h under ∼2 × 10^{-2} Torr of vacuum.

sinterability and reduce void formation. That is, higher powder loadings in the feedstock, and therefore higher green densities and greater particle-to-particle contact within the specimen, will yield less porosity and higher density in the final sintered body; a finding that agrees with results typically obtained in powder pressing studies [23].

Shown in Fig. 7(a) is an optical image of a sintered Ti-PIM tensile bar fabricated from feedstock initially containing 55 vol.% TiH_2. XRD and EDAX analyses indicate that the material is essentially pure α-Ti, which is consistent with the slow cooling rate that the specimen experienced after sintering. Two types of voids are apparent in this micrograph. The first are a set of large pores, typically >50 μm in size. Based on their size and shape, they appear to be the result of air bubbles that remained entrapped in the feedstock either after mixing or upon injection molding and can likely be eliminated with further process optimization. The observation of the second set of voids, much smaller in size (~10 μm) and more spherical in shape, suggested initially that sintering in this sample may have been prematurely interrupted. However, as shown in the etched image in Fig. 7(b) the majority of these pores are isolated within the grains of the material, indicating that the final stage of sintering is nearly complete.
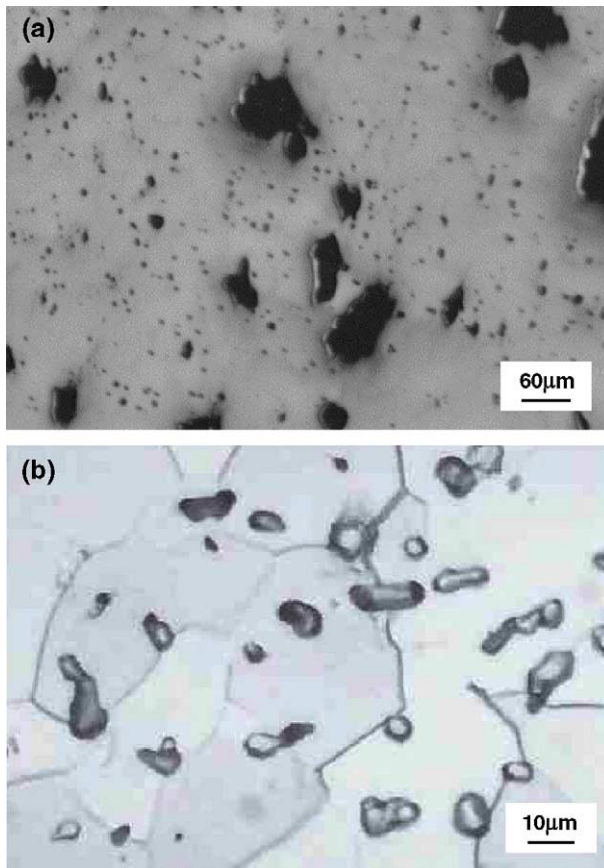

Fig. 7. Sintered microstructure of a PIM specimen prepared from feedstock initially containing 55 vol.% TiH_2 powder: (a) low magnification optical image and (b) high magnification optical image, etched condition.
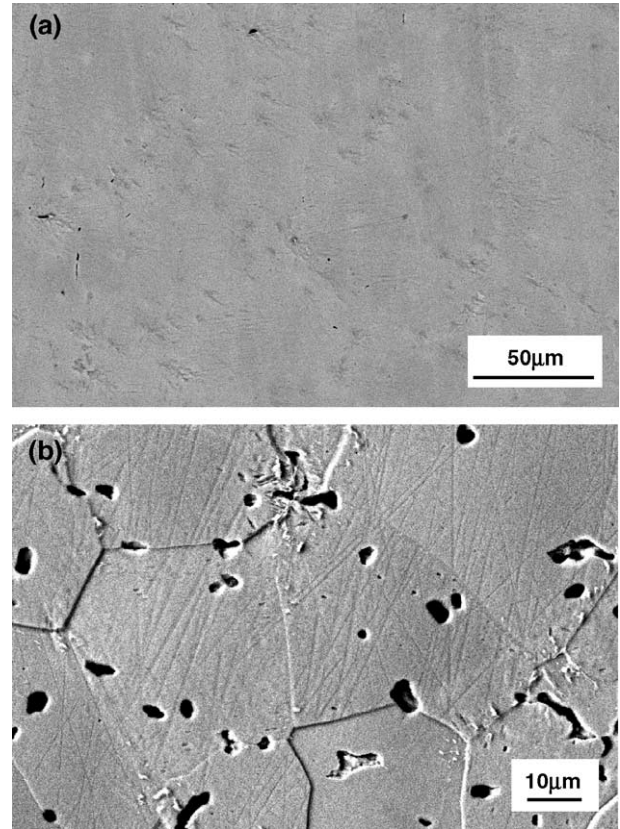

Fig. 8. Sintered microstructure of a PIM specimen prepared from feedstock initially containing 67 vol.% TiH_2 powder: (a) low magnification backscattered electron image and (b) high magnification backscattered electron image, etched condition.

The micrograph shown in Fig. 8(a) is of a sintered specimen fabricated from feedstock containing 67 vol.% TiH_2. Like the specimen in Fig. 7, this sample is also composed solely of α-Ti, but far fewer large flaws. In addition, the number of fine residual sintering pores is somewhat lower and their average size is measurably smaller, on the order of $3-5$ μm in size. The difference in these two microstructures reflects the densification results shown in Fig. 4, which as discussed previously originates
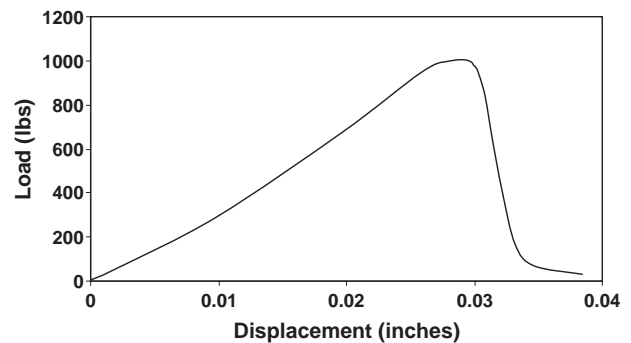

Fig. 9. Load–displacement curve obtained from tensile testing a sintered Ti-PIM specimen. The specimen was fabricated from feedstock initially containing 65 vol.% TiH_2 powder.
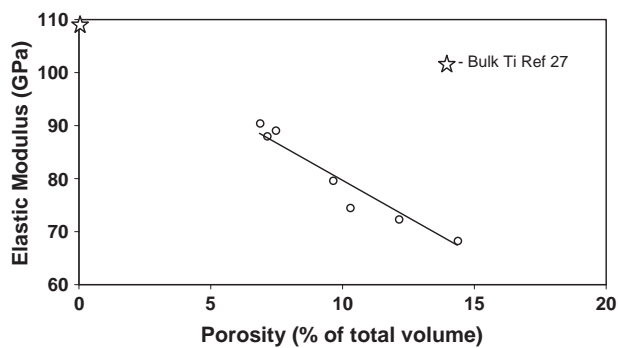
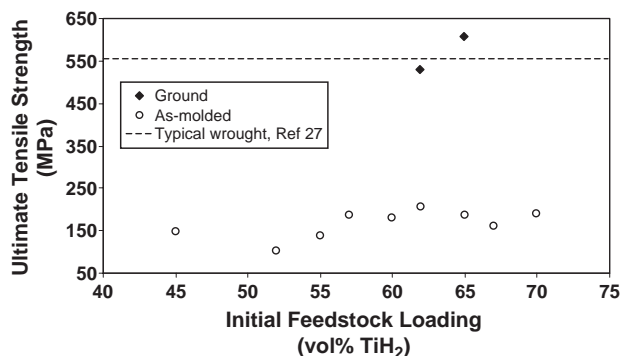Fig. 10. Elastic modulus versus volume fraction of porosity in the sintered Ti-PIM tensile specimens.

Fig. 11. Ultimate tensile strength of the sintered Ti-PIM tensile specimens as a function of initial feedstock loading.

from the dependence of green density on powder loading in the feedstock shown in Fig. 6.

Fig. 9 shows a typical load–displacement curve obtained from tensile testing, in this case of a 92.3% dense specimen fabricated from a 65 vol.% powder loaded feedstock. The curve displays linear elastic deformation followed by a small amount of plastic yielding and strain hardening up to a peak load. The subsequent drop in load is relatively rapid, indicating non-ductile behavior. Approximately 1–3% ductility was measured in the specimens, substantially lower than the 12–18% or higher levels generally exhibited by wrought α-Ti. As shown in Fig. 10, the elastic modulus of these specimens decreases linearly with increasing porosity, which agrees with results obtained by Oh et al. [24] and Ledbetter [25], and has potential significance in eventually using this process to designing an implant material with a stiffness matching that of natural bone. A lower titanium modulus may be desirable in that it allows greater load bearing contribution from the adjacent bone, which in turn helps to minimize atrophy and other undesirable interactions with the implant.

There appears to be several reasons for the reduced level of ductility observed in tensile testing. As indicated in Table 4, the original TiH_2 powder contains a significant amount of oxygen, which may be due to handling and storage under ambient conditions. Although the concentration of oxygen in the PIM specimens does not increase above that of the starting powder, it is substantially higher than the amount typically allowed in commercially pure titanium ($[O]_{max, Grade 1 Ti} = 0.1$ wt.%) [26]. Interstitial impurities such as oxygen, carbon, and nitrogen are tightly controlled in wrought product specifically because of their deleterious effect on ductility. Additionally, we observed molding flaws on the exterior surfaces of the specimens. These can act as

stress risers, causing premature failure in specimens already embrittled by α-Ti formation and high oxygen content.

To test this hypothesis, the gage section of several specimens was ground to a −10 μm finish on a lathe using sequentially finer grades of emery paper and the specimens were subsequently tensile tested. Plotted in Fig. 11 are the ultimate tensile strengths (UTS) of the specimens in both the as-ground and as-molded conditions as a function of TiH_2 loading in the initial feedstock material. Included for comparison is the average UTS of commercially pure titanium in the annealed condition. Note that the removal of the exterior molding flaws significantly improves the strength of the PIM material, which is slightly higher than wrought titanium. In addition, the ductility of these samples improves to 3–5%, although this is still only half of the desired value. Again, the higher levels of oxygen in the PIM materials are the likely cause of both higher strength and lower ductility relative to wrought product. The strength of the as-molded specimens is substantially lower than the ground specimens, indicating that the exterior molding flaws do play a significant role in these PIM-formed materials. It is anticipated that with process optimization, particularly in the feedstock mixing and injection molding steps, and the use of higher purity starting powder under inert conditions, the mechanical properties of titanium components made by this process will improve significantly. These studies are currently in progress.

4. Conclusions

In this study, a naphthalene-based method of titanium powder injection molding was used. Based on the results, the following conclusions were made:

- Sintered part density is directly related to the initial powder loading of the PIM feedstock. In order to maximize component density, high feedstock loadings should be employed. Conversely if increased porosity and pore size is desired, a lower powder loading can be used in the feedstock.

Table 4
Chemical analysis of starting powder and sintered Ti-PIM samples

Element analyzed	TiH_2 powder	PIM Sample 1	PIM Sample 2
C (ppm)	120	750	1470
N (ppm)	660	250	190
O (wt.%)	0.55	0.42	0.51

- The elastic modulus of these materials is inversely proportional to the concentration of inherent porosity.
- Virtually no additional oxygen impurities are introduced to the final sintered product using this Ti-PIM process.
- Tensile strengths equal to or higher than average wrought product can be obtained by this process. However in general, the Ti-PIM material exhibits lower ductility. Improvements in processing and powder chemistry are required to mitigate this problem.

Acknowledgments

References

[1] M. Niinomi, Metall. Mater. Trans. A 33 (2002) 477.
[2] J. Breme, V. Biehl, A. Hoffmann, Adv. Eng. Mater. 2 (2000) 270.
[3] F. Guillemot, F. Prima, R. Bareille, D. Gordin, T. Gloriant, M.C. Porte-Durrieu, D. Ansel, C. Baquey, Med. Biol. Eng. Comput. 42 (2004) 137.
[4] M. Niinomi, T. Hattori, K. Morikawa, T. Kasuga, A. Suzuki, H. Fukui, S. Niwa, Mater. Trans. 43 (2002) 2970.
[5] M. Niinomi, Sci. Technol. Adv. Mater. 4 (2003) 445.
[6] R. Van Noort, J. Mater. Sci. 22 (1987) 3801.
[7] R.M. German, Rev. Part. Mater. 1 (1993) 109.
[8] H.-H. Angermann, O. Van Der Biest, Mater. Manuf. Process. 10 (1995) 439.
[9] Y.S. Zu, Y.H. Chiou, S.T. Lin, J. Mater. Eng. Perform. 5 (1996) 609.
[10] C.T. Huang, K.S. Hwang, Powder Metall. 39 (1996) 119.
[11] C. Ouchi, H. Iizumi, S. Mitao, Mater. Sci. Eng., A 243 (1998) 186.
[12] Y. Kaneko, K. Ameyama, S. Sakaguchi, J. Jpn. Soc. Powder Metall. 37 (1990) 13.
[13] M.A. Ciomek, US Patent 5,064,463 (1991).
[14] H. Kyogoku, T. Toda, K. Shinohara, J. Jpn. Soc. Powder Metall. 40 (1993) 439.
[15] H. Wang, S.H.J. Lo, J.R. Barry, P/M Sci. Tech. Briefs 1 (5) (1999) 16.
[16] K. Kato, J. Jpn. Soc. Powder Metall. 46 (1999) 865.
[17] Nonprovisional patent application IP ID 14185-B, Battelle Memorial Institute.
[18] E. Nyberg, K. Simmons, K.S. Weil, in: T.R. Beiler, J.E. Carsley, H.L. Fraser, J.W. Sears, J.E. Smugeresky (Eds.), Trends in Materials and Manufacturing Technologies for Transportation Industries and Powder Metallurgy Research and Development in the Transportation Industry, TMS, Warrendale, PA, 2005.
[19] M.L. Wasz, F.R. Brotzen, B. McLellan, A.J. Griffin, J. Int. Mater. Rev. 41 (1996) 1.
[20] Y.T. Lee, H. Schurmann, K.-J. Grundhoff, M. Peters, Powder Metall. Int. 22 (1990) 11.
[21] R.M. German, A. Bose, Injection Molding of Metals and Ceramics, Metal Powder Industries Federation, Princeton, NJ, 1997.
[22] J. Fricke, A. Emmerling, J. Sol-Gel Sci. Technol. 13 (1998) 299.
[23] R.M. German, Metall. Trans. A 23 (1992) 1455.
[24] I.-H. Oh, N. Nomura, S. Masahashi, S. Hanada, Scr. Mater. 49 (2003) 1197.
[25] H. Ledbetter, Review of Progress in Quantitative Nondestructive Evaluation, Plenum Press, New York, 1995, p. 1663.
[26] Metals Handbook, 9th ed., American Society for Metals, Metals Park, OH, 1980, p. 372.
[27] M.J. Donachie Jr., Titanium: A Technical Guide, ASM International, Materials Park, OH, 2000.